Scientific Reports

https://doi.org/10.1038/s41598-026-45913-3

Article in Press

Designing a molecularly imprinted polymer sensor for sensitive and selective detection of the prostate cancer drug Abiraterone acetate

Received: 3 October 2025

Accepted: 23 March 2026

Published online: 29 April 2026

Cite this article as: Faysal A.A., Erdoğan T. & Gölcü A. Designing a molecularly imprinted polymer sensor for sensitive and selective detection of the prostate cancer drug Abiraterone acetate. *Sci Rep* (2026). https://doi.org/10.1038/s41598-026-45913-3

Abdullah Al Faysal, Taner Erdoğan & Ayşegül Gölcü

We are providing an unedited version of this manuscript to give early access to its findings. Before final publication, the manuscript will undergo further editing. Please note there may be errors present which affect the content, and all legal disclaimers apply.

If this paper is publishing under a Transparent Peer Review model then Peer Review reports will publish with the final article.

ARTICLE IN PRESS

© The Author(s) 2026. **Open Access** This article is licensed under a Creative Commons Attribution-NonCommercial-NoDerivatives 4.0 International License, which permits any non-commercial use, sharing, distribution and reproduction in any medium or format, as long as you give appropriate credit to the original author(s) and the source, provide a link to the Creative Commons licence, and indicate if you modified the licensed material. You do not have permission under this licence to share adapted material derived from this article or parts of it. The images or other third party material in this article are included in the article's Creative Commons licence, unless indicated otherwise in a credit line to the material. If material is not included in the article's Creative Commons licence and your intended use is not permitted by statutory regulation or exceeds the permitted use, you will need to obtain permission directly from the copyright holder. To view a copy of this licence, visit http://creativecommons.org/licenses/by-nc-nd/4.0/.

ARTICLE IN PRESS

Designing a Molecularly Imprinted Polymer Sensor for Sensitive and Selective Detection of the Prostate Cancer Drug Abiraterone Acetate

Abdullah Al Faysal[1], Taner Erdoğan[2], and Ayşegül Gölcü[1]*

[1]Istanbul Technical University, Faculty of Sciences and Letters, Department of Chemistry, Maslak, Istanbul, Türkiye.

[2]Kocaeli University, Kocaeli Vocational School, Department of Chemistry and Chemical Processing Technologies, Kocaeli, Türkiye

Abstract

This work has successfully implemented an electrochemical sensor based on molecularly imprinted polymers for the accurate and selective detection of abiraterone acetate (AA). AA serving as the template and 2-acrylamido-2-methyl-1-propane sulfonic acid acting as the functional monomer, in conjunction with other components essential for MIP formation, were used to fabricate the sensor through a photopolymerization technique, utilizing a glassy carbon electrode. Comprehensive characterizations of surface structure and electrochemical properties were conducted using scanning electron microscopy, atomic force microscopy, cyclic voltammetry, and Fourier transform infrared spectroscopy methods. Under optimized experimental conditions, the linear dynamic range of the developed sensor was established to be 1.0×10^{-12} to 1.5×10^{-11} M. The limits of detection and quantification for the sensor were established at the picomolar level, specifically 0.295 pM and 0.986 pM, respectively, demonstrating a linear response within the same concentration range when tested with commercial human serum samples. In both tablet and spiked serum samples, the relative standard deviations remained under 2.28%, and the AA recoveries varied between 97.84 and 103.83 %. Additionally, a series of Density Functional Theory calculations was conducted to better understand the experimental results and clarify the interactions between the template and monomer.

Keywords: Molecularly imprinted polymers, Abiraterone, Electrochemical sensor, Photopolymerization, Computational design

---

***Corresponding authors:** Prof. Ayşegül Gölcü, e-mail: aysgolcu@itu.edu.tr.

ARTICLE IN PRESS

ARTICLE IN PRESS

1. Introduction

Prostate cancer is the second most common solid tumor among men and the fifth leading cause of cancer-related deaths [1,2]. The outlook for advanced prostate cancer is usually poor, and its treatment presents significant difficulties. Within a timeframe of one to two years, this condition may evolve into castration-resistant prostate cancer (CRPC), which often subsequently advances to metastatic castration-resistant prostate cancer (mCRPC) [3]. The introduction of androgen deprivation therapy (ADT) in 1940 represented a major advance in treating metastatic prostate cancer and fundamentally changed its management. For people with metastatic prostate cancer, ADT is considered the primary treatment [1,4]. Even though ADT relieves most patients, a significant number eventually progress to CRPC and then to mCRPC [5,6]. mCRPC is a complex and aggressive condition characterized by varied responses to therapies targeting the androgen receptor signaling system. Patients diagnosed with this disease usually have a median survival time of less than three years [7,8]. Recent years have seen a major shift in how advanced prostate cancer is treated. Notably, the arrival of new hormonal therapies has become an important treatment choice for various stages of the disease [4,9]. Abiraterone acetate (AA), the prodrug of abiraterone, specifically and irreversibly inhibits CYP17, leading to a more significant reduction in androgen levels compared to isolated ADT [3,10]. AA is often used as the first treatment for mCRPC instead of more harmful options like docetaxel [11]. The combination of AA and a small amount of prednisone has been proven to improve survival in patients with mCRPC who have previously received treatment with docetaxel [12].

Several analytical techniques are currently established for measuring AA in bulk substances, dosage forms, and biological samples. These methods include spectrophotometry [13], spectrofluorimetry [14], high-performance liquid chromatography (HPLC) [15–17], HPLC-fluorescence [18,19], ultra-performance liquid chromatography-mass spectrometry (UPLC–MS/MS) [20], liquid chromatographic-tandem mass spectroscopy (LC–MS/MS) [21–24], and electroanalytical approaches [25]. Although these techniques are effective, they often require expensive equipment, hazardous solvents, and complex procedures, which limit their use and increase their environmental impact [26]. Electroanalytical methods have recently attracted significant interest from various academic fields. These techniques are notable for being highly sensitive, fast, cost-effective, easy to operate, and requiring minimal sample pretreatment. However, a significant challenge remains due to their limited selectivity, especially when

ARTICLE IN PRESS

analyzing analytes among metabolites or substances with similar molecular structures, such as enantiomers and degradation byproducts [27].

Molecular imprinting polymers (MIPs) use a self-assembly process to create customized binding sites, mainly through polymers [28]. MIPs demonstrate both specificity and affinity by targeting particular receptor sites designed to bind specific target molecules. This innovative approach has enabled the development of synthetic materials that mimic natural recognition mechanisms, allowing for the effective separation and identification of a wide range of chemical and biochemical substances [29]. MIPs have surpassed biological systems, especially in their improved sensitivity, specificity, and durability. These materials demonstrate exceptional stability under extreme conditions, enduring temperatures up to 150 °C and high pressures, while also resisting various harsh environments, including acids, bases, ions, and metals. A key feature of MIPs is their ability to maintain reactivity towards target analytes over extended periods, often allowing for effective storage without loss of performance [28,30]. MIP sensors have been utilized with various analyte measurement techniques, such as fluorescence [31], surface-enhanced raman scattering [32], surface plasmon resonance [33], and electrochemical methods [34]. Electrochemical sensing has gained notable attention as a superior method for detecting various molecules in biological samples compared to other techniques. This preference mainly stems from its benefits, including ease of use, fast response times, cost-effectiveness, and portability [35].

Numerous previous investigations have documented the development of MIP-based electrochemical sensors through photopolymerization, utilizing monomer systems akin to those employed in the current study. For instance, Tadi and Motghare [36] created MIP films on a carbon paste electrode aimed at determining pindolol. This was achieved through the free radical polymerization of itaconic acid, followed by cross-linking with ethylene glycol dimethacrylate. Similarly, Tadi et al. [37] conducted a theoretical analysis of the available functional monomers to identify the most appropriate functional monomer for the target template. Additionally, Faysal et al. [38] engineered an electrochemical sensor for acyclovir via UV-initiated polymerization of acrylamide and HEMA, which was cross-linked with EGDMA on a glassy carbon electrode. These instances illustrate that the development of photopolymerization-based MIP electrochemical sensors is ongoing. By integrating AMPS, which introduces sulfonic acid groups that may enhance ionic interactions, with well-optimized photopolymerization techniques, we are broadening the application of photopolymerized MIP sensors into novel chemical domains.

ARTICLE IN PRESS

In this study, we developed an electrochemical sensor using MIPs on a glassy carbon electrode (GCE) for AA detection. The sensor incorporated various MIP components, including 2-Acrylamido-2-methyl-1-propanesulfonic acid (AMPS) as the functional monomer, 2-hydroxyethyl methacrylate (HEMA) as the primary monomer, ethylene glycol dimethacrylate (EGDMA) as the cross-linker, and 2-hydroxy-2-methylpropiophenone as the UV initiator, all of which were integrated onto the GCE surface. A series of analytical techniques, including scanning electron microscopy (SEM), atomic force microscopy (AFM), Fourier transform infrared spectroscopy (FTIR), and cyclic voltammetry (CV), were used to evaluate the effectiveness and surface structure of the MIP. Despite the established nature of AMPS–EGDMA systems, it is essential to validate their applicability and the interactions between monomers and templates for each new analyte. We present both computational and experimental evidence that demonstrates AMPS engages in strong and selective interactions with AA, which facilitates a high imprinting efficiency. While photopolymerization is not a novel process, we have optimized the duration of photopolymerization, the ratios of monomers, and the thickness of the film to achieve a highly reproducible and stable MIP layer specifically designed for AA. In comparison to current electrochemical methods for AA, none of which utilize MIPs, our sensor provides lower detection limits, enhanced selectivity against structurally similar compounds, and a rapid response due to the thin photopolymerized MIP layer. We showcase dependable sensing capabilities in pharmaceutical formulations and spiked biological samples, underscoring a practical applicability that has not been documented previously for this analyte. Furthermore, the green profile score of the developed sensor was established by evaluating the Analytical Greenness Assessment Tool for Molecularly Imprinted Polymers Synthesis (AGREEMIP), the Analytical Greenness metric (AGREE), the Analytical Greenness preparation (AGREEprep), and the Blue Applicability Grade Index (BAGI).

2. Experimental

2.1. Reagents and chemicals

Istanbul University, Pharmaceutical Research Center supplied the active medicinal ingredients. The Devatis® 500 mg film-coated tablet was supplied by DEVA Holding at our request. Merck (Darmstadt, Germany) supplied the components HEMA (≥ 99.0%), EGDMA (≥ 98.0%), 2-hydroxy-2-methylpropiophenone (≥ 97.0%), and AMPS (99.0%). Additional reagents were obtained from Sigma-Aldrich (Darmstadt, Germany) and included potassium ferricyanide

ARTICLE IN PRESS

(≥99%), potassium ferrocyanide (≥99.0%), potassium chloride (≥99%), dopamine (DOP) (99.0%), ascorbic acid (≥99.0%), glacial acetic acid (HAc) (≥99.0%), uric acid (UA) (≥99.0%), potassium nitrate (≥99.0%), acetaminophen (PAR) (≥99.0%), acetone (99.5%), magnesium chloride (≥98.0%), methanol (MeOH) (99.9%), ethanol (EtOH) (≥99.50%), sodium sulfate (99.0%), acetonitrile (ACN) (99.9%), and human serum. Ultrapure water from the Milli-Q system (Merck, Guyancourt, France) was used to prepare all other chemicals in this study, which were of reagent grade. Ethanol and distilled water were used to prepare the stock solutions for AA (1 mM) and AMPS (1 mM), respectively. All of the stock and chemical solutions used in the study were stored in a refrigerator at approximately 4 °C to ensure their stability and reduce deterioration.

2.2. Instrumentation

The AUTOLAB PGSTAT302N potentiostat (Metrohm, Utrecht, Netherlands) was used for electrochemical tests. It was operated using NOVA 2.1.6 software in a three-electrode setup. This setup included a platinum wire as the auxiliary electrode, an Ag/AgCl reference electrode, and a 3.0 mm diameter MIP-modified GCE as the working electrode. Under specific conditions, such as a potential range of 0.0 to 0.8 V, a pulse width of 25 ms, a pulse amplitude of 25 mV, and a scan rate of 50 mV/s, the calibration curves and the analysis of actual samples were performed using differential pulse voltammetry (DPV).

The ATR-FTIR spectroscopy was recorded using an ATR-FTIR Shimadzu IRSpirit-T instrument (Shimadzu, Kyoto, Japan) with a resolution set at 2 cm^{-1} and a wavenumber range of 4000 to 650 cm^{-1}. SEM was used to visualize the MIP and NIP using a TESCAN GAIA 3 device (Brno-Kohoutovice, Czech Republic). A thermoshaker (TS-100, Biosan, Riga, Latvia) was employed to perform the template removal and reattachment procedure. Additionally, a UV lamp (B-100AP LAMP, Analytik Jena, Upland, CA, USA) was used to create the PP-MIP polymer layer.

2.3. Preparation of the MIP and NIP-based sensors

The preparation of the electrode surface is essential for the successful formation of the MIP film. First, the GCE is immersed in a mixture of equal parts distilled water and methanol, then treated in an ultrasonic bath for 15 minutes to ensure thorough cleaning. Next, the GCE is polished using an alumina slurry and a polishing pad, then rinsed with distilled water, and dried at room temperature. In a separate 2 mL Eppendorf tube, a solution is prepared by vortexing 20 µL of AA (1 mM) with 40 µL of AMPS (1 mM) for one minute. Then, 30 µL of HEMA and

ARTICLE IN PRESS

6 μL of EGDMA are added to this mixture, followed by vortexing for one minute to ensure complete mixing. Next, 20 μL of this mixture is separated, to which 1 μL of an initiator is added, and the solution is vortexed again for one minute. From this prepared solution, 0.5 μL—determined during optimization—are applied to the GCE surface. The photopolymerization process involves exposing the GCE to 365 nm UV light for five minutes, forming an MIP layer on the electrode surface. The electrode is then left to rest at room temperature for an additional 10 minutes. Subsequently, a removal process is performed to create cavities specific to AA within the PP-MIP(AA)/GCE sensor. During removal, the GCE is immersed in an Eppendorf tube containing a mixture of HAc and methanol in a 3:1 volume ratio. This setup is shaken on a ThermoShaker at 650 rpm for 12 minutes. For the rebinding phase, the same procedure is used; however, AA solutions at specified concentrations replace the removal solution, and this step lasts for 7 minutes. A non-imprinted polymer (NIP), which lacks specific binding sites, is prepared using the same steps but without AA in the photopolymerization solution. The resulting NIP/GCE is used to evaluate the selectivity and efficiency of the PP-MIP(AA)/GCE sensor. All electrochemical assessments are conducted with a 5.0 mM solution of the redox probe $[Fe(CN)_6]^{3-/4-}$, using an indirect measurement method.

2.4. Preparation of commercial serum and pharmaceutical samples

Five tablets of AA (Abiraterone Devaus®), each containing 500 mg of AA, were carefully ground and mixed. A precise amount of the resulting powder was weighed and added to a 50-mL volumetric flask, then dissolved to prepare a 1.0 mM AA solution in ethanol, followed by sonication for 15 minutes. Before measurement, the solution was diluted to the required concentration. The solution was stored at 4 °C in the dark to prevent any photochemical reactions.

To evaluate the relevance of the sensor for analyzing serum samples, a 3.6 mL commercial serum sample was mixed with 1.0 mL of an AA solution (1.0 mM) in a 10 mL centrifuge tube. Then, 5.4 mL of ACN was added, and the mixture was centrifuged at 5000 rpm for 25 minutes to precipitate proteins. After separating the supernatant, it was serially diluted to prepare a calibration curve.

The addition of known amounts of pure AA solution was used to perform recovery tests of AA in pharmaceutical and serum samples. The calibration curve's linear regression equation was employed to determine the amount of AA in the mixture. In every case, relative standard deviation (RSD) values were calculated using five different observations.

ARTICLE IN PRESS

2.5. Computational

In the computational part of the study, DFT calculations were performed to examine the nature of the interactions and the associated interaction energies between the template molecule and monomer molecules. DFT calculations have proven to be a powerful tool for obtaining valuable information regarding the structural stability and selectivity of MIP-based sensors [39]. DFT calculations with the use of B3LYP-D3 functional and 6-311G(d,p) basis set were performed on AA and AMPS. Calculations were carried out in the solution phase using the IEFPCM solvation model with water as the solvent. The geometry optimized structures of AA and AMPS were used to generate the initial structures of AA-AMPS complexes with template:monomer ratios ranging from 1:1 to 1:5. The initial structures obtained for each complex were further optimized using DFT calculations at the same level of theory. Furthermore, BSSE corrections were accounted for by conducting additional counterpoise calculations in the gas phase. Thus, the corresponding energies of the complexes (E_{comp}) were obtained. Then, the template molecule was removed from each structure, and the energy of the remaining system ($E_{monomer(s)}$) was recalculated. The same procedure was applied to the isolated template molecule to obtain the energy of the template ($E_{template}$). The interaction energies (ΔE) of the AA-AMPS complexes were obtained by the following formula:

$$\Delta E = E_{complex} - (E_{template} + E_{monomer(s)})$$

VeraChem Vconf [40], was used for conformational analysis, initial geometries of the template-monomer complexes were obtained using AutoDock Tools [41] and AutoDock Vina [42], DFT calculations were performed using Gaussian [43] and GaussView [44] and the results obtained were visualized using Discovery Studio Visualizer [45].

3. Results & discussion

3.1. Structural characterizations

The characterization of the chemical structures of the PP-MIP(AA)/GCE was performed using FTIR, as shown in **Figure 1A**. Overlapping peaks of the NH and OH functional groups cause a broad absorption band from 3100 to 3500 cm^{-1}. Also, the band at around 1508 cm^{-1} can be linked to the vibrational mode of the $-NH_2$ group. Moreover, the band at 1735 cm^{-1} indicates the presence of the C=O group associated with the monomers AMPS and HEMA. Characteristic peaks in the FTIR spectra of AMPS appeared at 1241 cm^{-1} due to the symmetric

ARTICLE IN PRESS

stretching of the S=O group and at 2924 cm^{-1} from the –CH stretching of $–CH_2$. The bands at 666 and 1011 cm^{-1} show the vibrational oscillation of S–O bonds and the symmetric oscillation of $−SO_2$ groups. These spectral features confirm that the SO_3H group is incorporated into the AMPS monomer. Based on these results, functional groups were successfully integrated into the surface of the film.

After the extraction of the template molecules, the absorption spectra of both the NIP (**Figure 1C**) and the MIP (**Figure 1B**) from which the template was removed, displayed a notable resemblance. This finding implies that the template molecules were successfully eliminated from the MIP matrix during the extraction procedure, resulting in the formation of specific recognition cavities while preserving the integrity of the overall polymeric structure. The similar spectral characteristics further suggest that the polymer backbone remained intact and that the imprinting process, along with the effective integration of the particles into the polymeric structure, was accomplished without causing any structural alterations in the polymer network. In order to facilitate a more precise comparison and enhance the depiction of the functional groups, the FTIR spectrum of the monomer AMPS has been incorporated in **Figure 1D**.

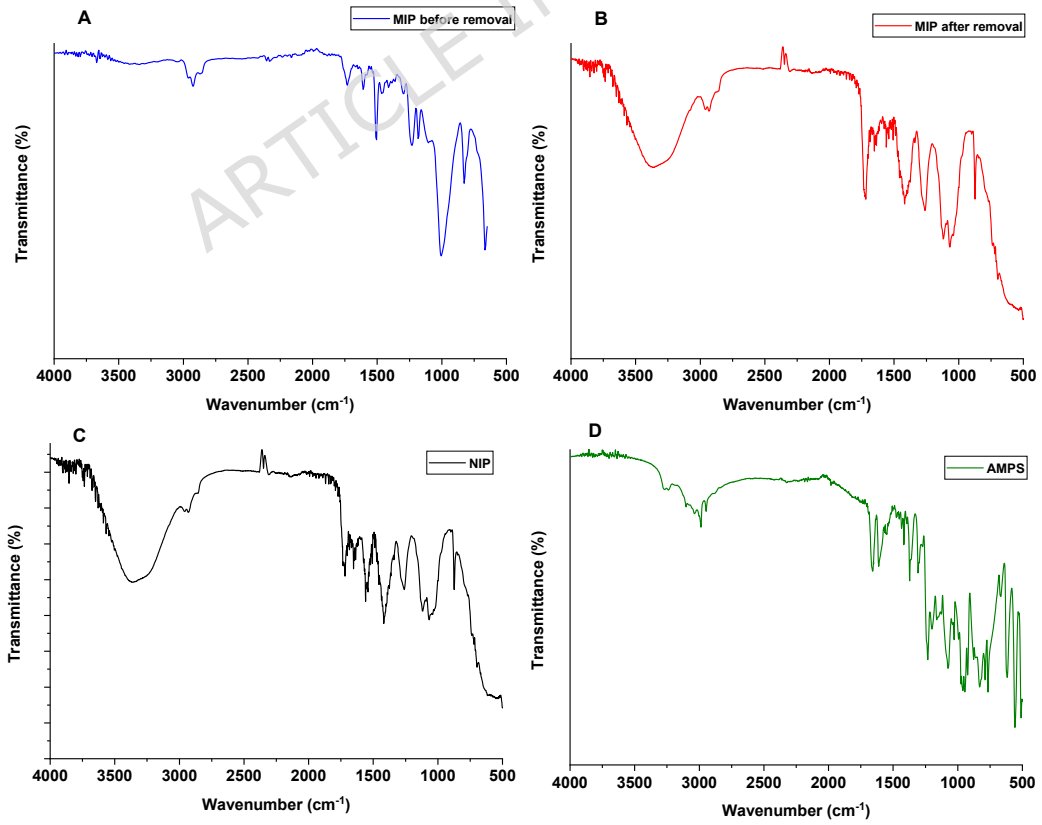

ARTICLE IN PRESS

Figure 1. FTIR spectra of (A) MIP before template removal, (B) MIP after template removal, (C) NIP surface, and (D) the monomer AMPS.

3.2 Surface characterization

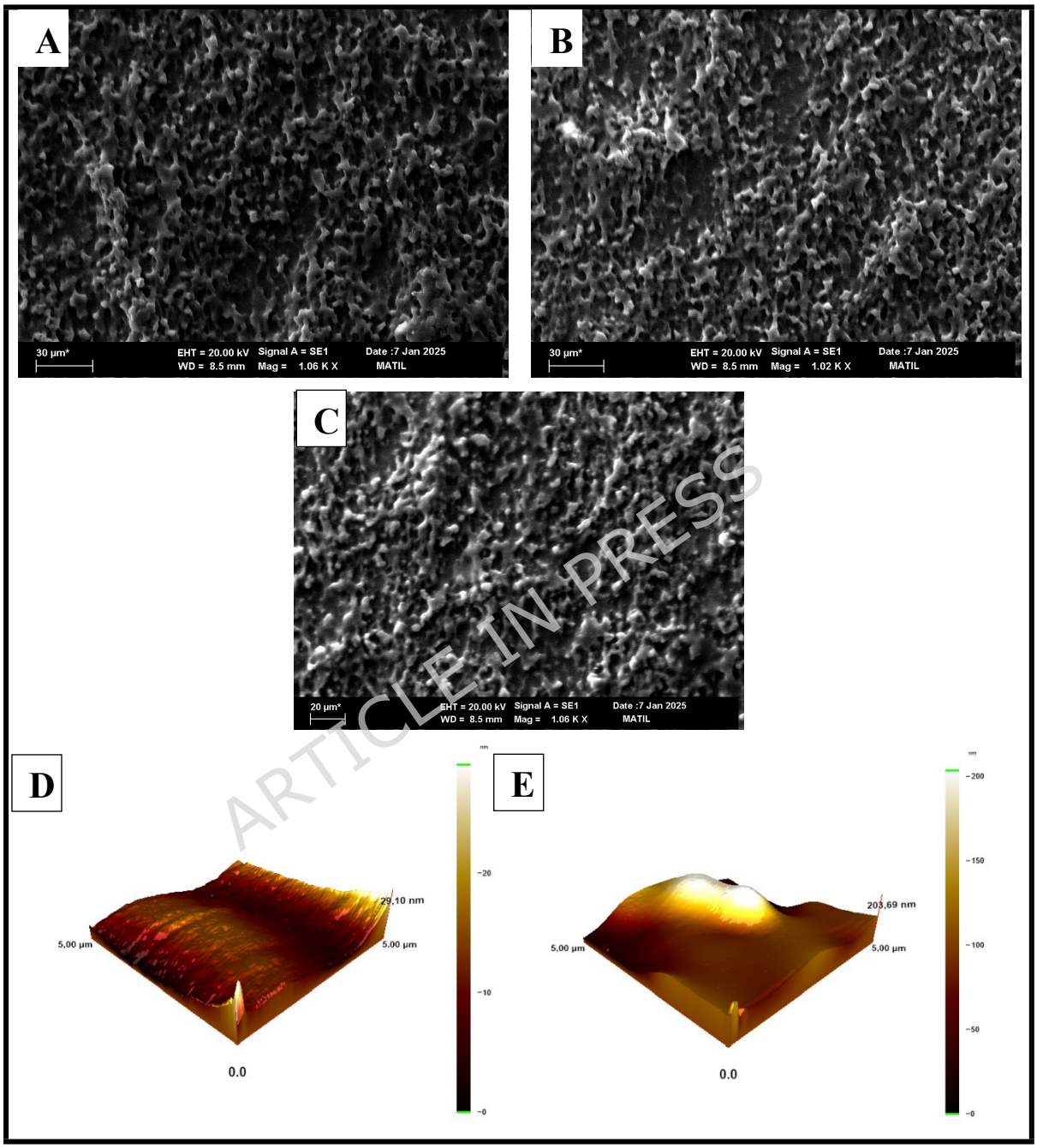

Figure 2. SEM images of the surfaces of **(A)** PP-MIP(AA)/GCE, **(B)** PP-MIP(AA)/GCE after removal, and **(C)** PP-NIP(AA)/GCE; and the AFM spectra of PP-MIP(AA)/GCE (**D**) MIP and (**E**) NIP.

ARTICLE IN PRESS

The surface properties of the manufactured sensors were analyzed through SEM analysis, as illustrated in **Figures 2A–C**. While the general morphologies of the modified electrodes seem largely similar at the chosen magnification, a detailed examination uncovers significant differences associated with the imprinting and template removal processes. The PP-MIP(AA)/GCE surface prior to template removal (**Figure 2A**) displays a relatively heterogeneous and compact polymeric texture that was developed during photopolymerization. Following the removal of the template (**Figure 2B**), the surface appears somewhat rougher, showcasing shallow cavities and void-like features, which indicate the successful extraction of the template molecules and the establishment of imprinted recognition sites. Conversely, the PP-NIP(AA)/GCE surface (**Figure 2C**) presents a more uniform and dense appearance, devoid of distinct cavity-like features due to the lack of a template during the polymerization process. Although the morphological distinctions are subtle, they align with the anticipated structural modifications brought about by molecular imprinting and corroborate the electrochemical findings that demonstrate the selective recognition capabilities of the MIP sensor.

AFM was employed to assess the surface morphology and roughness of both the imprinted and non-imprinted films. The AFM images depicted in **Figures 2D and 2E** represent the MIP and NIP layers, respectively. The film thickness measured for the MIP was 29.10 nm, in contrast to the NIP, which displayed a considerably greater thickness of 203.69 nm. The reduced thickness of the MIP can be attributed to the development of template-specific cavities during the polymerization process, leading to a more porous and less compact film when compared to the densely packed NIP layer. In a similar vein, the average roughness (R_a) values were recorded at 3.02 nm for the MIP and 30.86 nm for the NIP. The elevated roughness of the NIP indicates a more irregular and aggregated polymer surface, whereas the smoother topology of the MIP aligns with the presence of uniformly distributed imprinted cavities resulting from template removal. Collectively, these AFM findings validate the successful creation of MIP and NIP layers, each exhibiting distinct morphological features.

3.3. Electrochemical characterization of MIP/GCE sensor

The sensing mechanism of the proposed sensor is predicated on a modulation of electron transfer at the electrode interface, induced by template recognition. In this configuration, the electrochemical signal does not stem from the direct oxidation or reduction of AA. Rather, the signal is produced by the redox probe $[Fe(CN)_6]^{3-/4-}$, whose electron transfer dynamics are affected by the binding of the target molecule within the imprinted polymer matrix. During the

ARTICLE IN PRESS

fabrication of the sensor, photopolymerization occurs in the presence of the template molecule, leading to the creation of molecularly imprinted cavities that are complementary to AA in terms of size, shape, and orientation of functional groups. Following the removal of the template, these cavities remain accessible within the polymer network. When AA molecules are subsequently reintroduced into the system, they selectively rebind to these recognition sites through specific interactions with the functional groups present in the polymer matrix. The rebinding of AA within these cavities partially obstructs the diffusion pathways of the redox probe $[Fe(CN)_6]^{3-/4-}$ toward the electrode surface, thereby increasing the interfacial barrier for electron transfer. Consequently, the rate of electron transfer between the redox probe and the electrode diminishes, leading to a measurable reduction in the peak current observed during CV or DPV measurements. The extent of this current change is directly proportional to the concentration of AA present in the solution. Thus, the sensing mechanism is fundamentally based on the modulation of interfacial electron transfer induced by template recognition, wherein the selective rebinding of AA within the imprinted cavities modifies the accessibility of the electrode surface to the redox probe.

CV measurements were taken at different stages, including bare electrode, polymerization, removal, and rebinding, using a 5.0 mM redox probe, $[Fe(CN)_6]^{3-/4-}$ solution, to evaluate the electrochemical properties of the PP-MIP(AA)/GCE sensor. With each modification, the anodic and cathodic peak heights change, as shown in **Figure 3A**. The bare GCE surface exhibited the highest peak currents, due to the lack of barriers to electron transport, indicated by the red line. During the PP process, the anodic and cathodic peak currents of the redox probe decreased, which is expected and reflects the effectiveness of imprinting caused by limits in electron flow, as shown by the blue line. When the AA molecule was removed from the polymer matrix, specific cavities formed, resulting in an increase in the redox peak current, represented by the purple line. After controlled rebinding, the peak current decreased again, indicating that AA molecules could rebind to specific sites within the MIP sensor, as shown by the green line. **Figure 3B** illustrates a cyclic voltammogram that contrasts the sensing capabilities of bare electrodes, MIP, and NIP in a standard analyte solution. **Figure S1** illustrates the DP voltammogram responses obtained from a standard analyte solution at various stages of the fabrication process of the PP-MIP(AA)/GCE sensor. The peak current exhibits a decline post-polymer formation, followed by an increase after the removal of the template, attributed to the formation of imprinted cavities. Subsequently, there is another

ARTICLE IN PRESS

decrease in peak current upon analyte rebinding, thereby validating the successful fabrication of the sensor and its specific recognition capabilities.

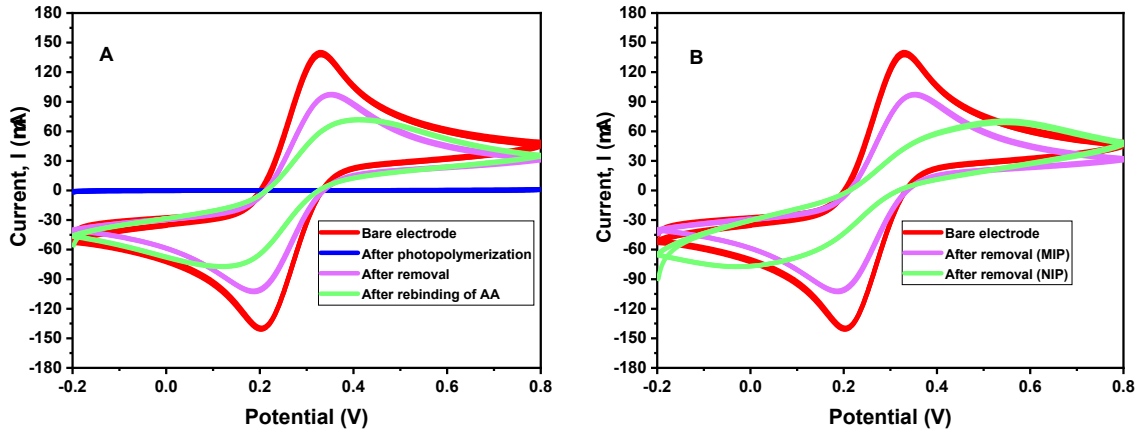

Figure 3. CV measurements in standard analyte solution (A) at each step of the developed PP-MIP(AA)/GCE sensor and (B) comparing the sensing response of bare, MIP-, and NIP-modified electrodes (Conditions for CV: potential scan range: −0.2 V to +0.8 V, scan rate: 0.05 V/s, step potential: 0.01 V).

3.4. Parameter optimization process of PP-MIP(AA)/GCE sensor

3.4.1. Functional monomer-to-template ratio

The interaction between the template molecule and the most compatible functional monomer is essential for forming a strong MIP network. The ratio of functional monomer to template must be adjusted appropriately to ensure effective interaction. If this ratio is not correctly set, the resulting polymer structure may fail to incorporate functional groups properly. These deficiencies can lead to issues such as reduced porosity and lower specificity in cavity formation. When the concentration of functional monomers exceeds the optimal level, they tend to distribute randomly within the polymer matrix rather than being incorporated selectively. To address these issues, we studied how different ratios affected the ΔIp_1 values, which measure the difference in peak currents before and after removal, as shown in **Figure S2A**. The results showed that the 1:2 ratio produced the best outcome, followed by a gradual decrease and stabilization in the values. Therefore, the 1:2 ratio was deemed most effective, and the polymerization solution was prepared based on this optimal ratio for the next experiments.

3.4.2. Dropping volume

ARTICLE IN PRESS

The amount of monomer solution needed to fully cover the GCE surface significantly affects the efficiency of polymerization. Additionally, the volume of solution used is closely related to both the thickness of the resulting polymer film and the length of the polymerization process. It is crucial to optimize the dropping volume to ensure the MIP film is deposited on the GCE surface as effectively as possible. In this study, different dropping volumes from 0.25 to 1.25 μL were tested to see how they impacted the sensor's performance, as shown in **Figure S2B**. The results showed that the ΔIp1 values varied with changes in the applied volumes, with the highest ΔIp1 observed at a dropping volume of 0.50 μL.

3.4.3. Photopolymerization (PP) time

The optimal duration for polymerization on the GCE surface is called the polymerization (PP) time. To improve the polymerization process under ultraviolet light exposure (365 nm, 100 W), experiments were performed over a range of 3 to 12 minutes. By comparing the PP time values to the related ΔIp_1, the best polymerization duration was determined. Results showed that 5 minutes produced the most significant, consistent, and reproducible results, as shown in **Figure S2C**.

3.4.4. Template removal solution and time

It is essential to preserve the polymeric layer when extracting template molecules from an MIP. This process creates specific cavities designed to bind the target analyte. Additional voids and channels also form, allowing the template to penetrate deeper into the MIP. This enhances the number of accessible cavities and improves the MIP's performance. Various elution solutions, such as EtOH, 15 M HAc, MeOH, and ACN, were tested in this study. Unfortunately, none of these solvents effectively removed the template molecule, leading to the exploration of different solvent mixtures as an alternative approach.

Upon investigating the impact of the removal process, it was observed that the ΔIp_1 values were significantly higher when using a mixture of HAc and MeOH in a 3:1 volume ratio, compared to the values recorded for other solvents and mixtures, as shown in **Figure S2D**. After selecting the removal solution, an optimization of the removal time was performed. To do this, various sensors were subjected to removal times ranging from 3 to 12 minutes, using a thermoshaker set at 650 rpm and 25 °C. The most consistent and reliable results were obtained at a removal time of 10 minutes, as shown in **Figure S2E**.

3.4.5. Rebinding time

Rebinding time optimization is crucial for evaluating the sensor's analytical efficiency. The sensor was tested using a thermoshaker and a 1.0×10^{-10} M AA solution at intervals from 3 to 12 minutes to identify the optimal rebinding time. The analysis focused on the difference in response between the extraction and rebinding stages (ΔIp_2) to determine the best conditions. Due to the rebinding of AA compounds to the imprinted sites, the observed ΔIp_2 values increased proportionally with time during the first 7 minutes, as shown in **Figure S2F**. After this time, only minor changes in response were observed, indicating that the imprinted sites reached saturation and equilibrium in the rebinding process. Therefore, a rebinding time of 7 minutes was deemed optimal and used in subsequent experiments.

3.5. Analytical performance of the MIP and NIP sensors

To demonstrate the analytical capability of the MIP/GCE, a comparative assessment between the MIP/GCE and NIP/GCE sensors was performed under optimal conditions, using a range of standard AA solution concentrations from 1.0×10^{-12} to 1.5×10^{-11} M (1–15 pM) with the DPV method. The resulting DPVs and their corresponding linear relationships are shown in **Figures 4A and 4B**, respectively. The linear relationship was determined by plotting the change in response, measured as ΔIp_2 values, before and after rebinding, against the AA concentrations. The calibration equation for the MIP/GCE sensor, ΔI (μA) = 3.11×10^{12} (μA/M) × C (M) + 49.81 (μA), demonstrated a strong correlation coefficient (r = 0.9982) (**Table 1**). Using the equations 3 × SD/Slope and 10 × SD/Slope [46], the LOD and LOQ values were calculated, resulting in 2.95×10^{-13} M and 9.86×10^{-13} M, respectively.

ARTICLE IN PRESS

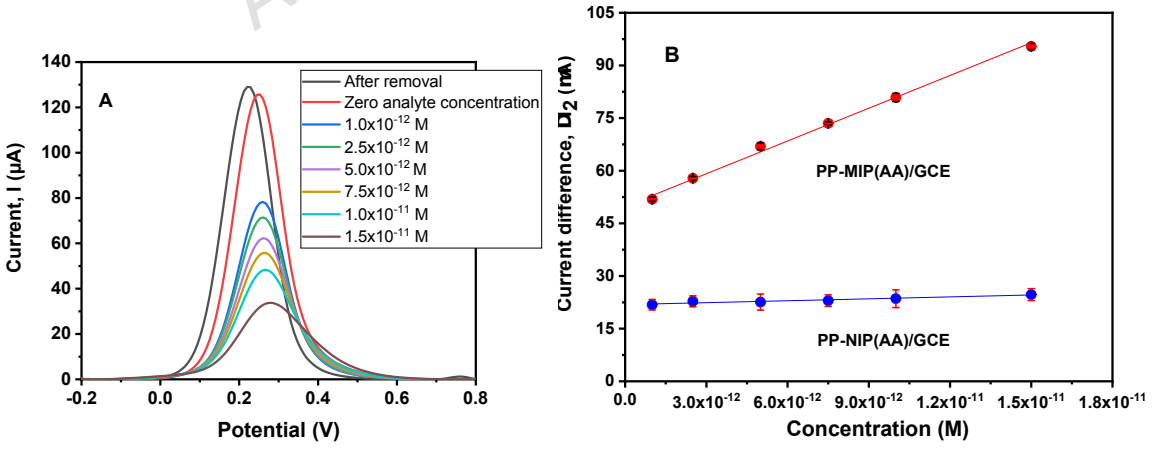

ARTICLE IN PRESS

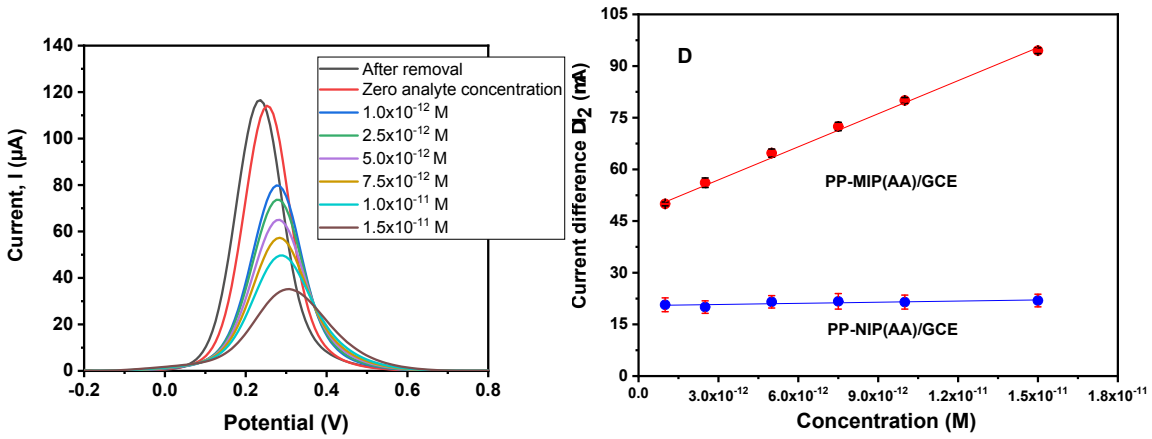

Figure 4. (A) DPVs of the MIP/GCE in comparison to the AA levels in the standard solution, and (C) spiked serum solution, **(B)** Linear relationships of the current difference (ΔIp_2) versus AA with MIP/GCE and NIP/GCE in standard solution, and **(D)** spiked serum solution (All measurements performed in 5.0 mM $[Fe(CN)_6]^{3-/4-}$ solution). (DPV Parameters; potential scan range, −0.2 to +0.8 V, scan rate 0.05 V/s, step potential 0.02 V, pulse amplitude 100 mV, modulation time 0.07 s).

Table 1. Regression parameters of AA on PP-MIP(AA)/GCE sensor.

	Standard solution	Commercial serum sample
Linearity range (M)	1.0×10^{-12} to 1.5×10^{-11}	1.0×10^{-12} to 1.5×10^{-11}
Slope (μA M^{-1})	3.11×10^{12}	3.20×10^{12}
SE of slope	6.37×10^{10}	6.57×10^{10}
Intercept (μA)	49.81	47.34
SE of intercept	0.43	0.54
Correlation coefficient (R)	0.9982	0.9988
LOD (M)	2.95×10^{-13}	2.66×10^{-13}
LOQ (M)	9.86×10^{-13}	8.87×10^{-13}
Repeatability of response (RSD%)*	0.58	0.55
Reproducibility of response (RSD%)**	1.14	1.49

*Each value is the mean of five experiments.

ARTICLE IN PRESS

**Repeatability and reproducibility studies were carried out at 1×10^{-12} M.

Table 2. DPV peak current differences (ΔI□) values at varying analyte concentrations in standard solutions and spiked serum samples.

	Standard solutions	Spiked serum samples
Concentration	**Difference (ΔI_2)**	**Difference (ΔI_2)**
	48.25	45.87
1.00E-12	48.60	46.06
	48.85	46.42
	54.83	52.02
2.50E-12	54.96	52.89
	54.41	53.61
	63.94	60.62
5.00E-12	64.82	61.90
	65.19	62.03
	70.46	68.34
7.50E-12	70.05	69.07
	69.83	70.11
	77.84	75.91
1.00E-11	75.98	76.40
	77.08	77.22
	92.38	90.35
1.50E-11	90.70	90.76
	91.56	91.87

As expected, the DPV signal for the NIP sensor showed little change as the template concentration increased. This behavior can be mainly explained by the NIP film's limited ability to recognize targets, which arises from its lack of imprinting spaces.

Since serum drug concentration is crucial for determining a drug's effectiveness and potential adverse effects, studying biological specimens, including serum, is very important for evaluating medicines. Using commercial serum samples spiked with AA across the concentration range of 1.0×10^{-12} to 1.5×10^{-12} M, the applicability of the manufactured MIP/GCE sensor was confirmed using the DPV approach (**Figure 4C**). An analogous validation was performed with the NIP/GCE, revealing the nonlinearity of the NIP compared

ARTICLE IN PRESS

to the MIP-based sensor (**Figure 4D**). For measuring AA in serum samples on MIP/GCE, the linear regression equation obtained was $\Delta I\ (\mu A) = 3.20 \times 10^{12}\ (\mu A/M) \times C\ (M) + 47.34\ (\mu A)$ ($r = 0.9988$). **Table 1** summarizes additional details regarding LOD, LOQ, and other validation parameters. **Table 2** illustrates the differences in DPV peak current (ΔI□) values across different analyte concentrations in both standard solutions and spiked serum samples.

3.6. Evaluation of the analytical performance of the PP-MIP(AA)/GCE sensor in commercial human serum and medicinal product samples

To evaluate the accuracy of the developed sensor using the serum sample, AA solutions were spiked at designated concentrations as part of a recovery study. According to the results shown in **Table 3**, the PP-MIP(AA)/GCE sensor exhibited high accuracy and practical functionality. In the next phase, pharmaceutical preparation samples were tested. Subsequently, an analysis of pharmaceutical product samples was conducted. The first step was to determine the labeled amount by analyzing the samples without any spiking, which showed that the detected amount was very close to the labeled amount. AA reference solutions were spiked into the tablet sample solution at specific concentrations to demonstrate the accuracy and suitability of the PP-MIP(AA)/GCE sensor.

Table 3. Recovery results for AA on PP-MIP(AA)/GCE.

	Abiraterone Devatis® tablet	Commercial serum sample
Label amount (mg)	500.00	-
Found amount (mg)*	509.97	-
RSD%*	2.79	-
Bias%	1.99	-
Spiked amount (mg)	10	10.00
Found amount (mg)*	10.02	10.27
Average recovery (%)	100.17	102.72
RSD% of recovery*	2.28	1.75
Bias%	0.17	2.72

*Each value is the mean of five experiments

3.7. Specificity and selectivity studies

The main goal of the investigations on the imprinting factor (k') was to analyze the key characteristics of PP-MIP(AA)/GCE, mainly focusing on selectivity and the accurate

ARTICLE IN PRESS

recognition of target molecules by MIP-based electrochemical sensors. It is crucial to assess the selectivity against structurally similar molecules, as the specific sites within the MIP framework are designed to match the chemical structure of the target molecule, AA. To do this, compounds that resemble the molecular structure of AA, along with other pharmaceuticals used in prostate cancer treatment, such as enzalutamide, darolutamide, olaparib, and niraparib (**Figure S3**), were used to calculate the values of k and the relative k (k').

An analysis of the sensor PP-MIP(AA)/GCE regarding the expected k' values in **Table 4** shows that the sensor displays both selectivity and a strong affinity for AA. Furthermore, the findings reveal that the sensor's selectivity for AA exceeds that of other chemical methods, reaching a selectivity ratio at least 2.24 times higher.

Table 4. The developed sensor's specificity for AA detection.

	PP-MIP(AA)/GCE		NIP		
	ΔI_2/µA	$k_{(MIP)}$	ΔI_2/µA	$k_{(NIP)}$	$k'_{(MIP/NIP)}$
AA	67.67	-	23.14	-	-
Enzalutamide	30.74	2.20	25.83	0.90	2.46
Darolutamide	28.61	2.37	26.63	0.87	2.72
Olaparib	35.11	1.93	26.91	0.86	2.24
Niraparib	32.04	2.11	26.47	0.87	2.42

ARTICLE IN PRESS

The reduced binding affinity observed in structurally analogous compounds can be ascribed to various molecular-level factors. Despite these analogues possessing certain steroidal characteristics akin to AA, their variations in steric geometry, size, and the orientation of substituents hinder their ability to fit accurately into the imprinted cavities formed during the polymerization process. The AMPS-based functional monomer engages in specific ionic and hydrogen-bonding interactions with AA throughout the imprinting phase. Analogues that do not possess the precise spatial configuration or functional groups required for complementary interaction are unable to achieve the same level of binding strength. As a result, they undergo diminished interaction within the cavities, which leads to a decrease in rebinding and a reduction in both imprinting and selectivity factors. This underscores the importance of structural specificity within the constructed MIP layer.

3.8. Evaluation of interference effect

ARTICLE IN PRESS

After establishing the sensor's functionality in a biological context, it is crucial to evaluate any potential interfering substances that may be present in such environments or introduced through absorption into the human body. This step ensures the PP-MIP(AA)/GCE sensor's ability to detect AA selectively remains unaffected. To assess its sensitivity to common compounds found in bodily fluids—such as K^+, Cl^-, Na^+, SO_4^{2-}, Mg^{2+}, Cl^-, dopamine (DOP), paracetamol (PAR), uric acid (UA), and ascorbic acid—the sensor's performance was tested. Selectivity was examined using the DPV technique, and percentage RSD and recovery values were calculated with tenfold higher concentrations of interferents compared to AA. The results shown in **Figure S4** demonstrate that the PP-MIP(AA)/GCE sensor can detect AA without interference from other substances. Additionally, as summarized in **Table S1**, the sensor effectively identifies AA while remaining unaffected by the presence of interferents.

3.9 Stability and reusability tests

Finally, the PP-MIP(AA)/GCE sensor was stored in a desiccator at ambient temperature for 15 days. Stability tests showed that the sensor stayed functional for up to 7 days, with performance metrics of 96.85% by the end of the 5th day, 91.62% at day 7, 78.58% after 10 days, and 65.83% at 15 days. As a result, the sensor's effective shelf life was determined to be 7 days, and its reusability was tested through 10 measurements taken after the rebinding process.

3.10. Comparison of selected analytical methods

The limitations observed in key characteristics such as selectivity, accuracy, and durability in current analytical methods are crucial in the ongoing search for new electrochemical sensors. Several studies have shown that using electrochemical techniques to evaluate pharmaceutical substances offers several advantages, including increased sensitivity, cost-effectiveness, simplicity, and quick detection. Selectivity is a vital feature of sensors that enables them to respond to analytes in complex matrices effectively. **Table 5** summarizes numerous studies conducted on the assessment of AA. The results of this research indicate that the sensors developed in this study demonstrate exceptional sensitivity for detecting AA. Compared to other methods, the findings emphasize beneficial features such as wide linearity, high reproducibility, low detection limits, specificity, and stability.

Table 5. Summary of selected analytical methods developed for AA.

Methodology	Linear range	LOD	Sample	Recovery (%)	Ref.

ARTICLE IN PRESS

Spectrophotometric	5–30 μg mL^{-1}	0.70 μg mL^{-1}	Tablets	98.57–100.48	[13]
Spectrofluorimetry	0.20 - 6.0 μg/mL	6.8 ng/mL	Tablet, serum and urine	98.23, 103.57, and 96.87	[14]
HPLC	1 - 100 μg.mL^{-1}	0.75 μg.mL^{-1}	Tablets	98.7 - 100.5	[16]
RP-UHPLC	0.5–20 μg/mL	0.1 μg/mL	Tablets	99.8− 101.2	[15]
UPLC–MS/MS	0.1–50 ng mL^{-1}	0.1ng mL^{-1}	Plasma	75.83–78.33%	[20]
LC–MS/MS	2–400 ng/mL	2 ng/mL	Serum	85.1–105.2%	[23]
LC–MS/MS	0.2–20 ng/mL	0.182 ng/mL	Plasma	-	[22]
cSPE/MWCNTs/CYP3A4	0 - 1 μM	230 nM	Serum	-	[25]
PP-MIP(AA)/GCE	1.0×10^{-12} - 1.5×10^{-11} M	0.29 pM	Tablet and serum	99.30 and 102.72	This study

ARTICLE IN PRESS

3.11. Green profile of the proposed sensor

The development of a green analytical method has become essential as an initial step towards implementing the principles of green chemistry in analytical research. In this context, alongside the optimization processes, we employed four matrices to select reagents and assess the environmental impact of our proposed method, aiming to reduce the amount of energy and chemicals required, as well as the waste generated. The principles of sustainability and ecological compatibility are crucial in the development of PP-MIP(AA)/GCE sensors.

ARTICLE IN PRESS

To evaluate the green profile score of the study, we utilized BAGI, AGREEprep, AGREE, and AGREEMIP. The numerical value displayed within the BAGI pictogram indicates the overall score assigned to the analytical method, which ranges from 25 to 100. A score of 25 indicates the poorest performance in terms of applicability.

For a method to be deemed feasible, it is suggested that it achieves a minimum of 60 points [47]. In the present study, a score of 77.5 was obtained (**Figure 5A**), demonstrating the applicability of the developed technique. The sensor's recyclability minimizes environmental impact and conserves resources. The principles of Green Analytical Chemistry (GAC) align with those of green chemistry, which generally advocate for a sustainable approach to the sensitive and selective determination of AA. A more user-friendly method is AGREEprep, which is based on ten categories of impact that were recalibrated to a 0–1 scale for sub-scores, subsequently utilized to compute the final assessment score.

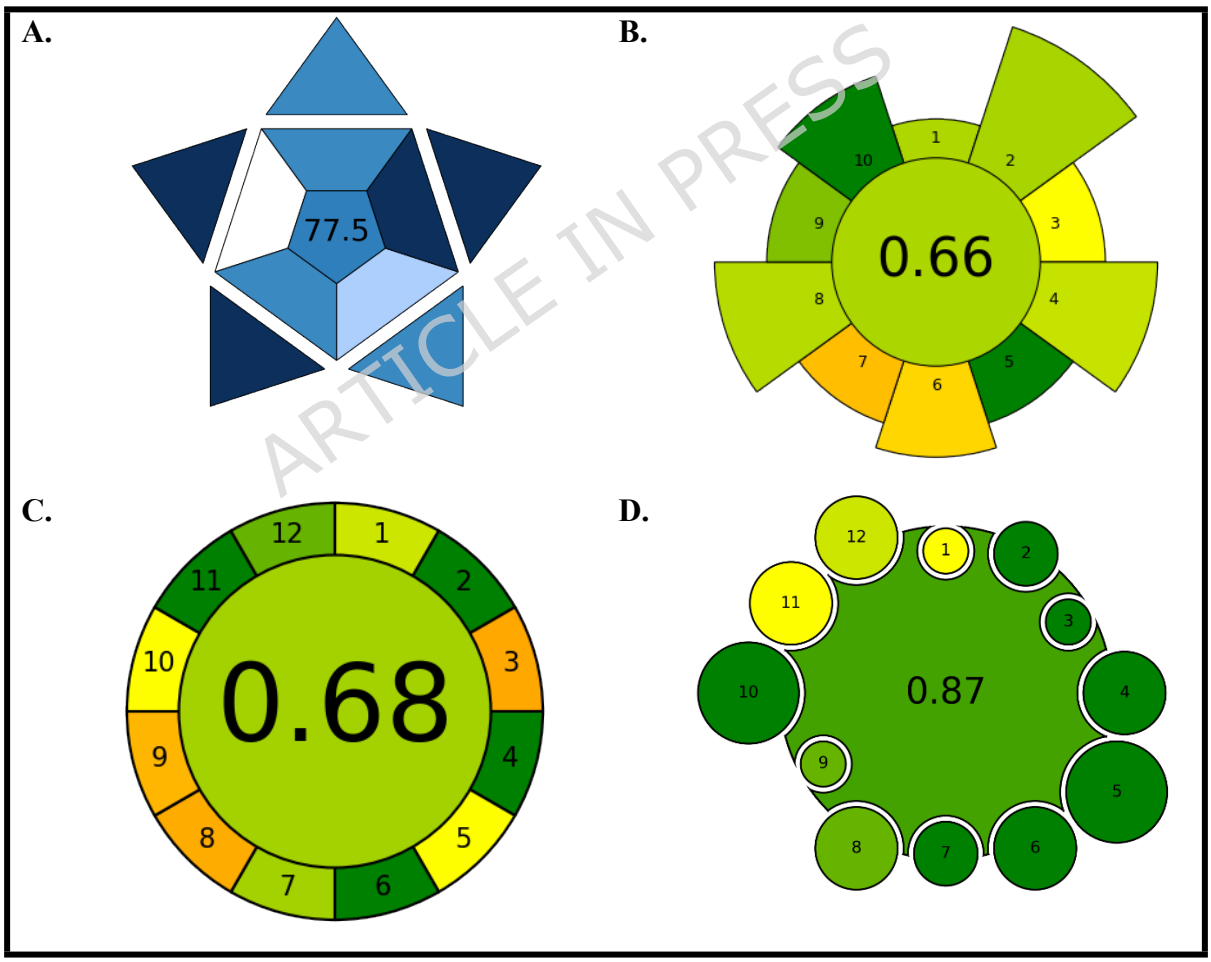

Figure 5. Pictograms for A) BAGI, B) AGREEprep, C) AGREE, and D) AGREEMIP.

ARTICLE IN PRESS

Strong performance is indicated by a score close to 1, whereas poor performance is indicated by a score close to 0 [48]. The present research's AGREEprep score was calculated to be 0.66, as shown in **Figure 5B**. This methodology shares both the benefits and drawbacks of the AGREE framework. The evaluation criteria of AGREE are derived from the 12 principles of GAC and are converted into a standardized 0–1 scale. A score approaching 0 reflects a lower level of environmental safety, whereas a score nearing 1 represents a higher level of sustainability [49]. Based on the findings from AGREE, the score for the current study was 0.68 (**Figure 5C**). This outcome indicates that less energy is utilized, and fewer hazardous chemicals are used. However, the approach faces some limitations, including the inability to conduct in situ analyses, partial automation, and the lack of integration of renewable resources. AGREEMIP is founded on twelve distinct assessment standards. The input data corresponding to these twelve criteria are converted into individual scores on a scale ranging from 0 to 1, which subsequently yield an overall score through the computation of the weighted average [50]. The results are displayed in an easily understandable pictogram that emphasizes the overall sustainability of the process along with the relevant weights. Considering that the AGREEMIP score for the present research was 0.87, the resulting sensor can be classified as highly green (**Figure 5D**). When assessing the environmental sustainability of MIP techniques, AGREEMIP proves to be a more effective GAC tool compared to alternative methods.

ARTICLE IN PRESS

3.12. Computational studies

Geometry-optimized structures of AA-AMPS complexes with template:monomer ratios from 1:1 to 1:5, obtained using the DFT approach with B3LYP-D3 functional and 6-311G(d,p) basis set, are shown in **Figure 6**.

ARTICLE IN PRESS

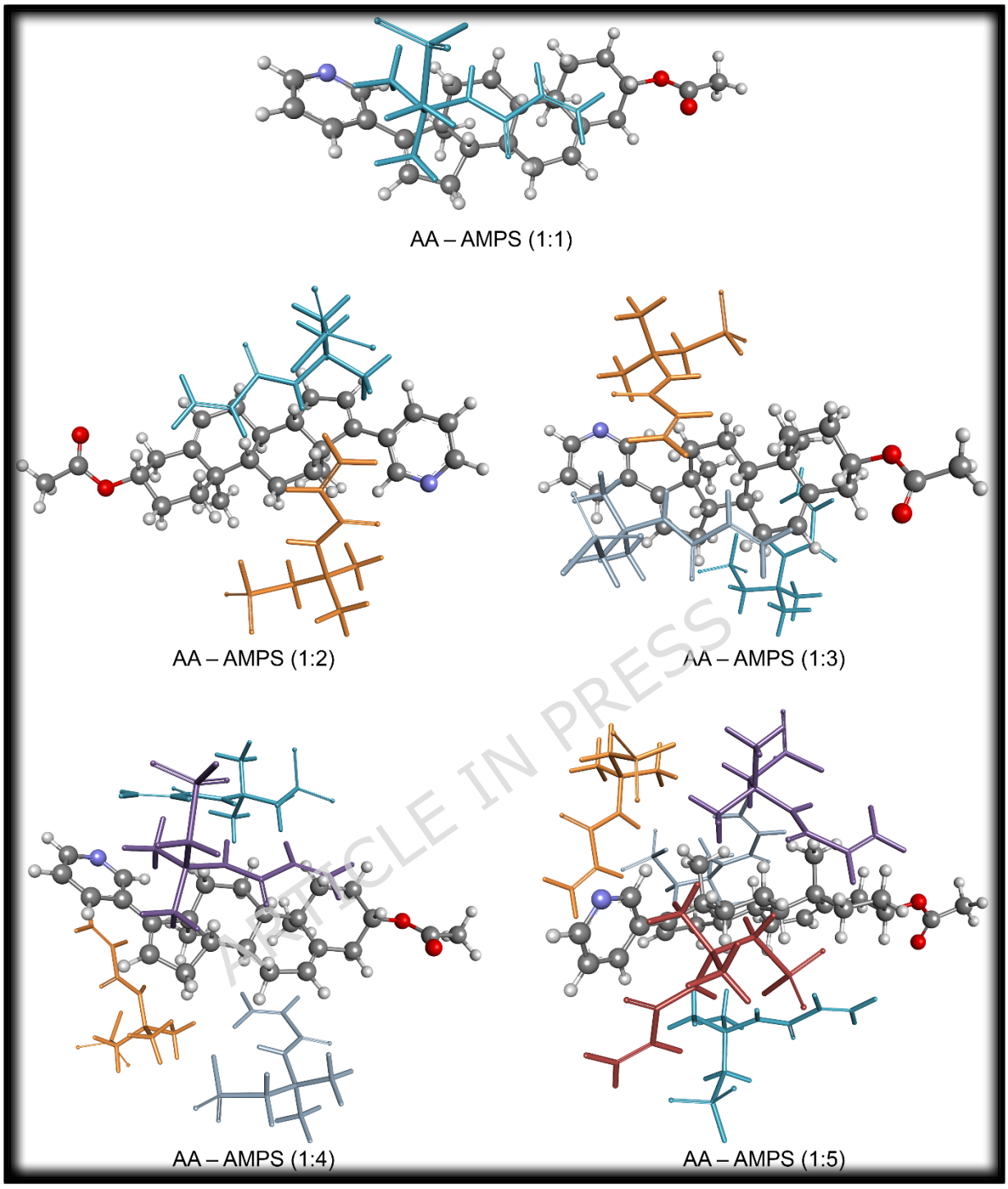

Figure 6. Geometry optimized structures belonging to AA-AMPS complexes.

The calculated interaction energies for the template-monomer complexes ranged from -35.75 kJ/mol to -89.29 kJ/mol (**Table S1**). As the template-to-monomer ratio increased from 1:1 to 1:4, a substantial increase in binding stability was observed, reaching a minimum of -89.29 kJ/mol at the 1:4 stoichiometry. However, the addition of a fifth monomer resulted in a less negative interaction energy (-74.45 kJ/mol), indicating a reduction in complex stability.

ARTICLE IN PRESS

In MIP-based sensors, insufficient interaction strength can lead to poor imprinting accuracy and weak template recognition, ultimately affecting the sensor's selectivity and sensitivity. On the other hand, overly strong interactions may hinder the effective removal of the template molecule during synthesis and reduce the reversibility of the recognition event during sensing. These issues are crucial for developing reusable and responsive systems. Therefore, maintaining a moderate yet adequate interaction strength is essential for achieving effective imprinting and dependable sensor performance.

In the computational analysis, the 1:1 complex exhibited a relatively weak interaction (-35.75 kJ/mol), which might be insufficient for maintaining the structural integrity of the imprinted cavity during polymerization. Conversely, the complexes with higher stoichiometries (1:3, 1:4, and 1:5) displayed significantly stronger interactions, reaching values as high as -89.29 kJ/mol. While such robust interactions may enhance sensitivity, they can simultaneously reduce selectivity and hinder effective template removal, thereby limiting the reversibility of the sensor. In contrast, the 1:2 complex demonstrated a moderate interaction strength of -53.33 kJ/mol. This value represents an ideal trade-off, providing sufficient stability for high-fidelity imprinting while ensuring high selectivity and facilitating efficient template extraction. Therefore, the 1:2 ratio is identified as the optimal configuration.

Experimental studies indicate that the sensor achieves its peak performance in terms of both selectivity and sensitivity at a 1:2 template-to-monomer ratio. This empirical finding aligns perfectly with our computational predictions. The calculated interaction strength for the 1:2 complex (-53.33 kJ/mol) falls within an ideal range; it is substantial enough to ensure the formation of a stable and selective cavity, yet sufficiently moderate to allow for effortless template removal and reversible recognition. Thus, the computational data reinforces the experimental choice of the 1:2 stoichiometry.

The interactions between template and monomer units for the complex with a 1:2 template:monomer ratio were also analyzed and are shown in **Figure S5**. Structural analysis of the optimized complexes reveals that the association between the template and the monomers is primarily driven by hydrophobic contacts. Specifically, alkyl and π-alkyl interactions were identified as the dominant non-covalent forces stabilizing the template-monomer interface. Furthermore, intramolecular hydrogen bonding was observed within the individual monomer units, which contributes to the conformational stability of the monomers in the complexed state.

4. Conclusion

ARTICLE IN PRESS

While prior studies have utilized APMS as a monomer for the preparation of MIP, our research introduces the first electrochemical approach based on MIP for the determination of AA, while also achieving significant enhancements in performance regarding detection limits and recovery accuracy. The sensing MIP was characterized morphologically and electrochemically using SEM, AFM, CV, and ATR-FTIR. The PP-MIP(AA)/GCE sensor demonstrated effective performance in detecting AA in both biological samples and standard solutions, showing specificity, quick analysis times, high sensitivity, and ease of use. The sensor exhibited exceptional linearity in standard solutions and biological matrices, along with notably low LOD and LOQ. The accuracy of the PP-MIP(AA)/GCE sensor was confirmed through recovery studies on serum samples spiked with AA and on tablet formulations. The findings suggest that the sensor has significant potential for monitoring drug concentrations in patients. Moreover, the sensor's ability to detect low concentrations and enable real-time monitoring suggests it could have broader applications in clinical diagnostics. The MIP/GCE sensor offers a useful opportunity for therapeutic drug monitoring by allowing accurate and continuous measurement of medication levels in patients' blood, which is crucial for personalized treatment. Additionally, this approach could be expanded to identify various pharmaceutical agents or biomarkers, providing valuable resources for pharmacokinetic research and disease diagnosis.

Acknowledgments

The authors would like to thank the support of the grant of Istanbul Technical University (Scientific Research Projects Unit) under the TGA-2023-45007 project. The computational studies reported in this paper were partially performed at TUBITAK ULAKBIM, High Performance and Grid Computing Center (TRUBA resources), and Kocaeli University (Kocaeli University Scientific Project Units, Project No: FBA-2023-3427). The authors gratefully acknowledge Ms. Zeynep Aydemir for her assistance in performing the FTIR experiments.

Author contributions

A.A.F.: Conceptualization, Methodology, Software, Writing - Original Draft, Investigation. **T.E.:** Investigation, Resources, Data Curation, Writing - Original Draft. **A.G.:** Supervision, Writing - Review & Editing, Project administration.

Funding

This study was not supported by any funding.

ARTICLE IN PRESS

ARTICLE IN PRESS

Clinical trial number

Not applicable.

Data availability statement

The datasets generated during and/or analyzed during the current study are available from the corresponding author upon reasonable request.

Ethical approval

This study does not require any ethical approval.

Competing Interests Statement

The author(s) declare no competing interests.

References

1. Chen, M. *et al.* Abiraterone, Orteronel, Enzalutamide and Docetaxel: Sequential or Combined Therapy? *Front Pharmacol* **13**, (2022).
2. Gandaglia, G. *et al.* Epidemiology and Prevention of Prostate Cancer. *Eur Urol Oncol* **4**, 877–892 (2021).
3. Wei, Z., Chen, C., Li, B., Li, Y. & Gu, H. Efficacy and Safety of Abiraterone Acetate and Enzalutamide for the Treatment of Metastatic Castration-Resistant Prostate Cancer: A Systematic Review and Meta-Analysis. *Front Oncol* **11**, (2021).
4. Lee, H. Y. *et al.* Abiraterone and enzalutamide had different adverse effects on the cardiovascular system: a systematic review with pairwise and network meta-analyses. *Prostate Cancer Prostatic Dis* **24**, 244–252 (2021).
5. Harris, A. E. *et al.* Exploring anti-androgen therapies in hormone dependent prostate cancer and new therapeutic routes for castration resistant prostate cancer. *Front Endocrinol (Lausanne)* **13**, (2022).
6. Crowley, F. *et al.* A Review of the Pathophysiological Mechanisms Underlying Castration-resistant Prostate Cancer. *Res Rep Urol* **Volume 13**, 457–472 (2021).
7. Nuhn, P. *et al.* Update on Systemic Prostate Cancer Therapies: Management of Metastatic Castration-resistant Prostate Cancer in the Era of Precision Oncology. *Eur Urol* **75**, 88–99 (2019).
8. Sweeney, C. *et al.* Ipatasertib plus abiraterone and prednisolone in metastatic castration-resistant prostate cancer (IPATential150): a multicentre, randomised, double-blind, phase 3 trial. *The Lancet* **398**, 131–142 (2021).

ARTICLE IN PRESS

ARTICLE IN PRESS

9. Clarke, N. W. *et al.* Abiraterone and Olaparib for Metastatic Castration-Resistant Prostate Cancer. *NEJM Evidence* **1**, (2022).

10. Choi, E., Buie, J. D., Camacho, J., Sharma, P. & de Riese, W. T. Evolution of Androgen Deprivation Therapy (ADT) and Its New Emerging Modalities in Prostate Cancer: An Update for Practicing Urologists, Clinicians and Medical Providers. *Res Rep Urol* **Volume 14**, 87–108 (2022).

11. La, J. *et al.* Abiraterone or Enzalutamide for Patients With Metastatic Castration-Resistant Prostate Cancer. *JAMA Netw Open* **7**, e2428444 (2024).

12. Ryan, C. J. *et al.* Abiraterone in Metastatic Prostate Cancer without Previous Chemotherapy. *New England Journal of Medicine* **368**, 138–148 (2013).

13. Akbel, E. Development, Validation, and Greenness Assessment of Eco-Friendly Analytical Methods for the Determination of Abiraterone Acetate in Pure Form and Pharmaceutical Formulations. *Separations* **11**, 290 (2024).

14. Gong, A. & Zhu, X. β-cyclodextrin Sensitized Spectrofluorimetry for the Determination of Abiraterone Acetate and Abiraterone. *J Fluoresc* **23**, 1279–1286 (2013).

15. Mhaske, D. K. & Kumbhar, A. S. The first RP-UHPLC method for simultaneous quantification of abiraterone acetate, its four degradants, and six specified process impurities and correct identification of all analytes based on molecular weight. *J Pharm Biomed Anal* **234**, 115568 (2023).

16. Beg, S. *et al.* Systematic Development and Validation of a RP-HPLC Method for Estimation of Abiraterone Acetate and its Degradation Products. *J Chromatogr Sci* **59**, 79–87 (2021).

17. Kavitapu, D., Maruthapillai, A., Mahapatra, S. & Arockia Selvi, J. New stability indicating RP-HPLC method for the determination of Abiraterone acetate, its related substances and degradation products in bulk and dosage form. *Mater Today Proc* **34**, 469–478 (2021).

18. Rodriguez, J., Castaneda, G., Lizcano, I. & Villa, J. C. A Rapid, Direct and Validated HPLC- Fluorescence Method for the Quantification of Abiraterone and Abiraterone Acetate in Urine and Serum Samples from Patients with Castration- Resistant Prostate Cancer. *Curr Pharm Anal* **14**, 233–238 (2018).

19. Belleville, T. *et al.* A HPLC-fluorescence method for the quantification of abiraterone in plasma from patients with metastatic castration-resistant prostate cancer. *Journal of Chromatography B* **989**, 86–90 (2015).

20. Wani, T. A. Highly sensitive ultra-performance liquid chromatography–tandem mass spectrometry method for the determination of abiraterone in human plasma. *Analytical Methods* **5**, 3693 (2013).

21. van Nuland, M., Hillebrand, M. J. X., Rosing, H., Schellens, J. H. M. & Beijnen, J. H. Development and Validation of an LC-MS/MS Method for the

ARTICLE IN PRESS

Simultaneous Quantification of Abiraterone, Enzalutamide, and Their Major Metabolites in Human Plasma. *Ther Drug Monit* **39**, 243–251 (2017).

22. van Nuland, M. *et al.* An LC–MS/MS method for quantification of the active abiraterone metabolite Δ(4)-abiraterone (D4A) in human plasma. *Journal of Chromatography B* **1068–1069**, 119–124 (2017).

23. Alyamani, M. *et al.* Development and validation of a novel LC–MS/MS method for simultaneous determination of abiraterone and its seven steroidal metabolites in human serum: Innovation in separation of diastereoisomers without use of a chiral column. *J Steroid Biochem Mol Biol* **172**, 231–239 (2017).

24. Caron, P., Turcotte, V., Lévesque, E. & Guillemette, C. An LC-MS/MS method for quantification of abiraterone, its active metabolites D(4)-abiraterone (D4A) and 5α-abiraterone, and their inactive glucuronide derivatives. *Journal of Chromatography B* **1104**, 249–255 (2019).

25. Aliakbarinodehi, N., De Micheli, G. & Carrara, S. Highly Sensitive Enzymatic MWCNTs-Based Biosensors for Detection of Abiraterone in Human Serum. *Bionanoscience* **8**, 675–679 (2018).

26. Karimi-Maleh, H., Karimi, F., Alizadeh, M. & Sanati, A. L. Electrochemical Sensors, a Bright Future in the Fabrication of Portable Kits in Analytical Systems. *The Chemical Record* **20**, 682–692 (2020).

27. Motaharian, A., Naseri, K., Mehrpour, O. & Shoeibi, S. Electrochemical determination of atypical antipsychotic drug quetiapine using nano-molecularly imprinted polymer modified carbon paste electrode. *Anal Chim Acta* **1097**, 214–221 (2020).

28. Basak, S., Venkatram, R. & Singhal, R. S. Recent advances in the application of molecularly imprinted polymers (MIPs) in food analysis. *Food Control* **139**, 109074 (2022).

29. Parisi, O. I. *et al.* The Evolution of Molecular Recognition: From Antibodies to Molecularly Imprinted Polymers (MIPs) as Artificial Counterpart. *J Funct Biomater* **13**, 12 (2022).

30. Wang, W. *et al.* Recent advances in nanomaterials-based electrochemical (bio)sensors for pesticides detection. *TrAC Trends in Analytical Chemistry* **132**, 116041 (2020).

31. Murugan, K., Jothi, V. K., Rajaram, A. & Natarajan, A. Novel Metal-Free Fluorescent Sensor Based on Molecularly Imprinted Polymer N-CDs@MIP for Highly Selective Detection of TNP. *ACS Omega* **7**, 1368–1379 (2022).

32. Hu, Y. & Lu, X. Rapid Detection of Melamine in Tap Water and Milk Using Conjugated “One-Step” Molecularly Imprinted Polymers-Surface Enhanced Raman Spectroscopic Sensor. *J Food Sci* **81**, (2016).

33. Ertürk Bergdahl, G. *et al. In Vivo* Detection and Absolute Quantification of a Secreted Bacterial Factor from Skin Using Molecularly Imprinted Polymers in a Surface Plasmon Resonance Biosensor for Improved Diagnostic Abilities. *ACS Sens* **4**, 717–725 (2019).

ARTICLE IN PRESS

ARTICLE IN PRESS

34. El-Wekil, M. M., Halby, H. M., Darweesh, M., Ali, M. E. & Ali, R. An innovative dual recognition aptasensor for specific detection of Staphylococcus aureus based on Au/Fe3O4 binary hybrid. *Sci Rep* **12**, 12502 (2022).

35. Wang, L., Pagett, M. & Zhang, W. Molecularly imprinted polymer (MIP) based electrochemical sensors and their recent advances in health applications. *Sensors and Actuators Reports* **5**, 100153 (2023).

36. Tadi, K. K. & Motghare, R. V. Voltammetric Determination of Pindolol in Biological Fluids Using Molecularly Imprinted Polymer Based Biomimetic Sensor. *J Electrochem Soc* **163**, B286–B292 (2016).

37. Tadi, K. K., Motghare, R. V. & Ganesh, V. Electrochemical detection of epinephrine using a biomimic made up of hemin modified molecularly imprinted microspheres. *RSC Adv* **5**, 99115–99124 (2015).

38. Al Faysal, A. *et al.* Development and Fabrication of a Molecularly Imprinted Polymer-Based Electroanalytical Sensor for the Determination of Acyclovir. *ACS Omega* **9**, 9564–9576 (2024).

39. Tadi, K. K. & Motghare, R. V. Rational synthesis of pindolol imprinted polymer by non-covalent protocol based on computational approach. *J Mol Model* **19**, 3385–3396 (2013).

40. Chang, C.-E. & Gilson, M. K. Tork: Conformational analysis method for molecules and complexes. *J Comput Chem* **24**, 1987–1998 (2003).

41. Morris, G. M. *et al.* AutoDock4 and AutoDockTools4: Automated docking with selective receptor flexibility. *J Comput Chem* **30**, 2785–2791 (2009).

42. Trott, O. & Olson, A. J. AutoDock Vina: Improving the speed and accuracy of docking with a new scoring function, efficient optimization, and multithreading. *J Comput Chem* **31**, 455–461 (2010).

43. Frisch, M. J. *et al.* Gaussian 16 Revision C.01. Preprint at (2016).

44. Roy Dennington, Todd A. Keith & John M. Millam. GaussView 6. Preprint at (2016).

45. BIOVIA, Discovery Studio Visualizer. Preprint at (2023).

46. Ozkan, S. A., Kauffmann, J.-M. & Zuman, P. *Electroanalysis in Biomedical and Pharmaceutical Sciences*. (Springer Berlin Heidelberg, Berlin, Heidelberg, 2015). doi:10.1007/978-3-662-47138-8.

47. Manousi, N., Wojnowski, W., Płotka-Wasylka, J. & Samanidou, V. Blue applicability grade index (BAGI) and software: a new tool for the evaluation of method practicality. *Green Chemistry* **25**, 7598–7604 (2023).

48. Wojnowski, W., Tobiszewski, M., Pena-Pereira, F. & Psillakis, E. AGREEprep – Analytical greenness metric for sample preparation. *TrAC Trends in Analytical Chemistry* **149**, 116553 (2022).

49. Pena-Pereira, F., Wojnowski, W. & Tobiszewski, M. AGREE—Analytical GREEnness Metric Approach and Software. *Anal Chem* **92**, 10076–10082 (2020).

ARTICLE IN PRESS

ARTICLE IN PRESS

50. Marć, M., Wojnowski, W., Pena-Pereira, F., Tobiszewski, M. & Martín-Esteban, A. AGREEMIP: The Analytical Greenness Assessment Tool for Molecularly Imprinted Polymers Synthesis. *ACS Sustain Chem Eng* **12**, 12516–12524 (2024).

ARTICLE IN PRESS